



Regional-scale
transport of air
pollutants

J. Li et al.

This discussion paper is/has been under review for the journal Atmospheric Chemistry and Physics (ACP). Please refer to the corresponding final paper in ACP if available.

Regional-scale transport of air pollutants: impacts of southern California emissions on Phoenix ground-level ozone concentrations

J. Li¹, M. Georgescu^{1,2}, P. Hyde³, A. Mahalov¹, and M. Moustaoui¹

¹Julie Ann Wrigley Global Institute of Sustainability, School of Mathematical and Statistical Sciences, Arizona State University, Tempe, AZ 85287, USA

²School of Geographical Sciences and Urban Planning, Arizona State University, Tempe, AZ 85287, USA

³School for Engineering of Matter, Transport and Energy, Arizona State University, Tempe, AZ 85287, USA

Received: 15 January 2015 – Accepted: 26 February 2015 – Published: 19 March 2015

Correspondence to: J. Li (jialun.li@asu.edu)

Published by Copernicus Publications on behalf of the European Geosciences Union.

Title Page

Abstract

Introduction

Conclusions

References

Tables

Figures



Back

Close

Full Screen / Esc

Printer-friendly Version

Interactive Discussion



Abstract

In this study, WRF-Chem is utilized at high-resolution (1.333 km grid spacing for the innermost domain) to investigate impacts of southern California anthropogenic emissions (SoCal) on Phoenix ground-level ozone concentrations ($[O_3]$) for a pair of recent exceedance episodes. First, WRF-Chem Control simulations are conducted to evaluate model performance. Compared with surface observations of hourly ozone, CO, NO_x , and wind fields, the Control simulations reproduce observed variability well. Simulated $[O_3]$ are within acceptance ranges recommended by the Environmental Protection Agency (EPA) that characterize skillful experiments. Next, the relative contribution of SoCal and Arizona local anthropogenic emissions (AZ) to ozone exceedance within the Phoenix metropolitan area is investigated via a trio of sensitivity simulations: (1) SoCal emissions are excluded, with all other emissions as in Control; (2) AZ emissions are excluded with all other emissions as in Control; and (3) SoCal and AZ emissions are excluded (i.e., all anthropogenic emissions are eliminated) to account only for biogenic emissions [BEO]. Results for the selected events indicate the impacts of AZ emissions are dominant on daily maximum 8 h average (DMA8) $[O_3]$ in Phoenix. SoCal contributions to DMA8 $[O_3]$ for the Phoenix metropolitan area range from a few ppbv to over 30 ppbv (10–30% relative to Control experiments). $[O_3]$ from SoCal and AZ emissions exhibit the expected diurnal characteristics that are determined by physical and photochemical processes, while BEO contributions to DMA8 $[O_3]$ in Phoenix also play a key role. Finally, ozone transport processes and pathways within the lower troposphere are investigated. During daytime, pollutants (mainly ozone) near the southern California coasts are pumped into the planetary boundary-layer over the southern California desert through the mountain chimney and pass channel effects, aiding eastward transport along the desert air basins in southern California and finally, northeastward along the Gila River basin in Arizona, thereby affecting Phoenix air quality during subsequent days. This study indicates that local emission controls in Phoenix need to be

Regional-scale transport of air pollutants

J. Li et al.

Title Page

Abstract

Introduction

Conclusions

References

Tables

Figures



Back

Close

Full Screen / Esc

Printer-friendly Version

Interactive Discussion



augmented with regional emission reductions to attain the federal ozone standard, especially if a more stringent standard is adopted in future years.

1 Introduction

Tropospheric ozone is a strong oxidant controlling much of the chemistry in the atmosphere, such as hydroxyl production and the lifetimes of atmospheric species (see review in He et al., 2013). Tropospheric ozone is also a greenhouse gas and acts as the important anthropogenic contributor to radiative forcing of climate (IPCC, 2007). Lower tropospheric ozone adversely affects human health (Anderson, 2009; Smith et al., 2009), reduces crop yields (Avnery et al., 2011; Chameides et al., 1999), and damages natural ecosystems (Ashmore, 2005; Mauzeral and Wang, 2001). Therefore, ozone (O_3) is one of the six criteria pollutants regulated by the US Environmental Protection Agency (EPA) through National Ambient Air Quality Standards (NAAQS). The current NAAQS for O_3 concentrations ($[O_3]$) is 75 ppbv, defined as the 3 year average of the annual fourth-highest daily maximum 8 h average (DMA8) $[O_3]$ for each monitoring site within an airshed. The US EPA has already proposed to lower the standard to 65–70 ppbv (EPA 2014) and may also redefine the national O_3 secondary standard for protecting sensitive vegetation and ecosystems (Huang et al., 2013). Currently, many US cities are classified as NAAQS O_3 nonattainment areas based on the 2008 federal standard (<http://www.epa.gov/airquality/greenbook/hnc.html>). In addition, sensitive areas (e.g., national parks and wilderness areas) also experience DMA8 O_3 exceedances (<http://www.nature.nps.gov/air/Monitoring/exceed.cfm>). Therefore, improved understanding and attribution of $[O_3]$ sources in these areas is necessary to develop effective air quality management strategies to achieve ever more stringent US air quality standards.

As a secondary pollutant, measured ground-level $[O_3]$ is the result of O_3 production/loss due to local sources of precursor emissions, to transport of O_3 and its precursors from nearby and/or remote regions, and to ozone formed from natural precursor

Regional-scale transport of air pollutants

J. Li et al.

Title Page

Abstract

Introduction

Conclusions

References

Tables

Figures



Back

Close

Full Screen / Esc

Printer-friendly Version

Interactive Discussion



emissions. The direct way to characterize O₃ source attribution is through field measurements (e.g., Fast et al., 2002; Kemball-Cook et al., 2009; Nunnermacker et al., 2004). The other way to identify transported O₃ and local generated O₃ is to use trajectory models (e.g., MacDonald et al., 2006; Lanford et al., 2010).

5 Transport of ozone and its precursors from one area to another is determined by flow patterns, which can be obtained by measurement and/or modeling. However, information on flow alone is insufficient in ozone studies because of the complexity of chemistry involved, wherein ozone and precursors nonlinearly interact with flow, turbulence and sunlight to determine ozone distributions (Huang et al., 2013; Lee et al., 2003, 2007; Levy II et al., 1985). Chemical transport models (CTMs) are increasingly common in simulating atmospheric chemical and transport processes at regional/continental/global scales because of the detailed physical and chemical processes being implemented. For example, using a CTM (GFDL AM3), Lin et al. (2012) found that Asian O₃ pollutants can affect surface [O₃] in the western US, contributing up to 8–15 ppbv to the DMA8; and that Asian pollution increase the DMA8 O₃ exceedance days by 53% in the southwestern US. Huang et al. (2013), combining model simulations at 12 km resolution (WRF/STEM), remote-sensing, and ground-based observations, have studied the effect of southern California anthropogenic emissions (SoCal) on ozone pollution in southwestern US mountain states. They found that the SoCal precursor emissions and its transported ozone increase [O₃] up to 15 ppbv in western Arizona. They also characterized the nonlinear relationship between emissions and [O₃]. However, these studies have not examined the impacts of regional emissions on [O₃] in an urban setting (such as Phoenix), at high-resolution.

25 Physical/chemical-based CTM modeling is the only available tool for ozone transport predictions on finer spatial scales (Lee et al., 2007). Many studies have investigated ozone transport at urban scales using coupled meteorological and chemistry models. For example, Lu et al. (1997) found that ozone and other pollutant concentrations were higher in northern and eastern Los Angeles (LA) than those in the western and central Greater LA, where strong emission sources are located, due to transport owing to

Regional-scale transport of air pollutants

J. Li et al.

Title Page

Abstract

Introduction

Conclusions

References

Tables

Figures



Back

Close

Full Screen / Esc

Printer-friendly Version

Interactive Discussion



**Regional-scale
transport of air
pollutants**

J. Li et al.

Title Page

Abstract

Introduction

Conclusions

References

Tables

Figures



Back

Close

Full Screen / Esc

Printer-friendly Version

Interactive Discussion



the persistent onshore sea breeze and mountain-induced upslope flow. Analogously, that surface $[O_3]$ in the Phoenix metropolitan area and its rural environs are higher in northeastern than in southwestern Phoenix arises from transport of urban pollutants by prevailing southwest winds (Fast et al., 2000; Lee et al., 2003, 2007; Lee and Fernando, 2013). Although these studies have considered both chemistry and transport processes at the urban scale, they did not try to distinguish between ozone produced by local emissions and that produced by regional transport, a principal motivation of this study.

The Phoenix metropolitan area is classified as an O_3 nonattainment area under the 2008 NAAQS primary O_3 standard (<http://www.epa.gov/airquality/greenbook/hnc.html>). Therefore, it is helpful to separately quantify the relative contributions of local emissions and regional transport to Phoenix $[O_3]$ in order to design feasible and effective ozone control strategies. Both aircraft observations (Nunnermacker et al., 2004) and backward trajectory analysis (MacDonald et al., 2006) indicate that surface $[O_3]$ on exceedance days are attributed to both Arizona local anthropogenic emissions (AZ) and regional and/or continental transport. Therefore, our focus is to use a CTM to separately quantify the contributions of local and regional emissions to the ozone distributions in Phoenix on exceedance days, research which has not been published in peer-reviewed journals.

In addition, previous studies indicate that coarse-resolution modeling cannot adequately represent the heterogeneities of ozone and meteorological fields in Phoenix due to its complex terrain (Fast et al., 2000; Lee et al., 2003; Lee and Fernando, 2013). That high-resolution CTMs can obtain better results in modeling urban air quality is also reported for the LA basin, Mexico City, and other regions (e.g., Tie et al., 2010; Chen et al., 2013; Lu and Turco, 1995, 1996; Taha, 2008; Klich and Fuelberg, 2014; Stock et al., 2014). Therefore, employing a high-resolution CTM to address air pollutant distributions in the Phoenix metropolitan area due to local emissions and regional transport is our second motivation.

**Regional-scale
transport of air
pollutants**

J. Li et al.

Title Page

Abstract

Introduction

Conclusions

References

Tables

Figures



Back

Close

Full Screen / Esc

Printer-friendly Version

Interactive Discussion



Using WRF-Chem (Grell et al., 2005) at high-resolution, we will examine: (1) the relative contributions of SoCal and AZ to the ozone episodes in Phoenix, and (2) how SoCal (emissions) affect Phoenix $[O_3]$. This is a topic that has received limited research attention to date (Moore, 2014), but requires investigation because of the metropolitan area's non-attainment ozone status and because of the need to evaluate the effectiveness of local anthropogenic emission control strategies necessary to attain the standard.

2 Methodology

2.1 WRF-Chem setup

We use WRF-Chem as the integration CTM since it has been successfully used in this region (Chen et al., 2011; Li et al., 2014; Zhao et al., 2012). In WRF-Chem, the Weather Research and Forecast (WRF) model (Skamarock et al., 2008) is employed to resolve atmospheric physics and dynamical processes, while the coupled chemistry (Chem) model is used to simulate chemical processes such as gaseous and aqueous chemical reactions, dispersion, and deposition. The WRF-Chem setup includes the Lin's cloud scheme (Lin et al., 1983), the RRTM radiation scheme (Mlawer et al., 1997), the Noah land surface model with single layer urban canopy model (Chen and Dudhia, 2001; Chen et al., 2011; Ek et al., 2003), the Grell-Devenyi ensemble cumulus scheme (Grell and Devenyi, 2002) that allows subsidence and spreading at high-resolution, a revised MM5 surface layer, and the BouLac Planetary Boundary Layer (PBL) schemes. Land cover and land use data from the MODIS 1 km resolution dataset (Friendl et al., 2002) are combined with the 2006 National Land Cover Database (NLCD) 3 class urban covers to better represent the urban landscape. The second generation regional acid deposition model (RADM2, Stockwell et al., 1990; Gross and Stockwell, 2003) is used for gas-phase chemical reactions. The aerosol algorithms are based on the MADE/SORGAM (Ackermann et al., 1998; Shell et al., 2001) with GOCART, functioning as an emission scheme that accounts for surface wind speed, soil moisture, and

soil erodibility (Ginoux et al., 2001; Zhao et al., 2010). The other selected chemistry schemes are based on the recommendations provided in the WRF-Chem users' guide (Peckam et al., 2013).

Four nested domains are used (Fig. 1a). The first (domain 1) has 36 km grid spacing and covers the western and central US, eastern Pacific, northern and central Mexico, the Gulf of California, and the western Gulf of Mexico. Nested domains 2, 3, and 4 use grid spacings of 12, 4, and 1.333 km, respectively. The innermost domain (1.333 km) grid spacing (with 640 by 301 grid cells) encompasses southern California (the Southern Coast Air Basin–SCAB or Greater Los Angeles Air Basin–GLABS, the San Diego Air Basin or SDAB, the southern Mojave Desert Air Basin or SMDAB, the Salton Sea Air Basin or SSAB, and the southern part of the South Central Air Basin. See Fig. 1b), and central and southern Arizona to better represent the complex terrain and land cover features (see Fig. 1b). As shown in Fig. 1b, the mountainous features in southern California and Arizona are well represented at high resolution. The San Gorgonio Pass (between the San Bernardino Mountains and the San Jacinto Mountains), the Cajon Pass (between the San Gabriel Mountains and the San Bernardino Mountains), and the Newhall Pass (west of the San Gabriel Mountains) are also resolved. The observation sites (including O₃, NO_x, CO, and surface wind observations) used for validation of the Control simulations are also superimposed (Fig. 1b).

2.2 Data used for model initialization and evaluation

The biogenic emission data are obtained from the 1 km resolution Model of Emissions of Gases and Aerosols from Nature (MEGAN, Guenther et al., 2006). The North American Regional Reanalysis (NARR; Mesinger et al., 2006) product is used for initial and boundary conditions (atmospheric and land surface (e.g., soil moisture and temperature)). NARR data are distributed on a 32 km grid with a 3 h temporal frequency. The atmospheric chemical boundary and initial conditions are obtained from the global air quality forecast model called MOZART-4/GEOS-5 (https:

Regional-scale transport of air pollutants

J. Li et al.

Title Page

Abstract

Introduction

Conclusions

References

Tables

Figures



Back

Close

Full Screen / Esc

Printer-friendly Version

Interactive Discussion



//www2.acd.ucar.edu/acresp/forecasts), available on a $1.9^\circ \times 2.5^\circ$ grid (Emmons et al., 2010).

The anthropogenic emissions used in this study are obtained from 2005 National Emissions Inventories (NEI05) data provided by the U.S. EPA (www.epa.gov/ttnchie1/net/2005inventory.html). These data are distributed on a 4 km grid array covering the US and surrounding land areas. A method utilized to interpolate the 4 km grid spacing NEI05 data to any resolution one wishes to use for WRF-Chem simulations is provided with the WRF-Chem system (http://www.acd.ucar.edu/wrf-chem/). Each WRF-Chem model grid point data is based on averaging from those NEI05 grid points that fall within a distance less than the WRF-Chem model resolution. The method works well when WRF-Chem grid spacing is coarser than 4 km. However, the method misrepresents emissions when the model resolution is greater than the NEI05 grid. To overcome this issue, we have used Monotonic Cubic Interpolation to downscale the 4 km resolution NEI05 data to a 1.333 km resolution grid (the finest model grid spacing of our WRF-Chem simulations). Details on the NEI05 downscaling method and improved simulation performance are discussed separately (Li et al., 2014).

The data used for model evaluation include measurements of surface wind speed and direction (24 sites within Domain 4). These wind fields are obtained from two networks: the AZMET (ag.arizona.edu/azmet), and the Air Quality and Meteorological Information System (AQMIS) in the California EPA/Air Resources Board (www.arb.ca.gov/aqmis2/aqmis2.php). We use hourly observations of ozone concentrations from 26 stations in Arizona (downloaded from www.epa.gov/ttn/airs/airsaqs/) and 46 stations in Southern California (downloaded from www.arb.ca.gov/aqmis2/aqdselect.php?tab=hourly). In addition, the hourly NO_x observations, including four stations in Arizona and over 20 sites in southern California, and hourly CO observations, including four stations in Arizona and about 20 stations in southern California, can be obtained from the same websites as ozone data. Comparison of simulated and observed VOC concentrations was precluded by the latter's irregular availability and their lack of hourly concentrations.

Regional-scale transport of air pollutants

J. Li et al.

Title Page

Abstract

Introduction

Conclusions

References

Tables

Figures



Back

Close

Full Screen / Esc

Printer-friendly Version

Interactive Discussion



2012 and 16–19 July 2005. These comparisons, which indicate sufficiently faithful and accurate meteorological simulations, ensure that regional pollutant transport can be adequately simulated, one of our focuses in this study. No vertical wind comparisons are made since WRF-Chem is driven by NARR, into which the sounding information has already been assimilated (Mesinger et al., 2006).

Figure 3 shows the comparison of CO, NO_x, and O₃ concentrations between the model (bold-red, i.e., CTRL run) and observations (bold-black) in Domain 4 for the same time periods. On average, the model performed well for both CO and NO_x concentrations for the July case. In contrast, for the May case, the model overestimated CO and NO_x during nighttime but matched observations during daytime. The standard deviations (thin-red) from the model are much greater than those from observations (thin-black), indicating that modeled NO_x and CO heterogeneity at sites is greater than that from observations. The model behavior in the May case indicates that the anthropogenic emissions could be over-estimated using the NEI05 data due to emission control strategies enacted in California in the seven intervening years (Pusede and Cohen, 2012). How much the NEI05 emissions should be reduced in southern California depends on the CTM model employed. For example, Chen et al. (2013), in simulating LA air quality in May 2010, found that by reducing NO_x emissions by 45 %, WRF-Chem O₃ and NO_x concentrations matched the observations best, compared with reducing emissions by 24 %. For simulating the same time periods, Huang et al. (2013), using WRF/STEM, found that model simulations and observations matched well by reducing NO_x emissions of the NEI05 by 20 %.

The [O₃] comparison between observations and simulations presented in Fig. 3 indicates the model performed better in simulating [O₃] than CO or NO_x. Both the station average and station standard deviation from model and observations matched each other on event and non-event days (detail on site-by-site comparisons in Phoenix will be discussed in the next section). The simulated average [O₃] and their spatial heterogeneities fall within the ranges of observations except on 13 May 2012, when modeled average [O₃] and the spatial standard deviations fall out of the observation ranges.

Regional-scale transport of air pollutants

J. Li et al.

[Title Page](#)[Abstract](#)[Introduction](#)[Conclusions](#)[References](#)[Tables](#)[Figures](#)[Back](#)[Close](#)[Full Screen / Esc](#)[Printer-friendly Version](#)[Interactive Discussion](#)

5 areas (ID9508, ID9702). AZ emissions are the main source contribution to ozone production over Phoenix during daytime (compare the change in simulated $[O_3]$ as demonstrated by the red contour (CTRL) and blue contour (noAZ)), with a maximum magnitude of up to 40–60 ppbv hourly (compare differences between CTRL and noAZ). The contribution of SoCal emissions to Phoenix $[O_3]$ ranges between 10–40 ppbv during daytime (compare the change in simulated $[O_3]$ as demonstrated by the red contour (CTRL) and green contour (noCA)). Based on the BEO run (gray contour), the contribution of biogenic emissions (including larger-scale lateral input) to Phoenix $[O_3]$ varies between 25–35 ppbv, indicating a baseline target for emission reduction strategies.

10 Figure 4 indicates the relative contribution of SoCal and AZ emissions to $[O_3]$ vary with time. Physical and chemical processes at each stage can explain this variation. During nighttime, noCA experiment $[O_3]$ is less than that of noAZ run. This is because there is no ozone consumption (or titration) in the noAZ run while transported ozone can still make its contribution. After sunrise, solar radiation heats the ground surface, increasing planetary boundary layer (PBL) height. Ozone accumulated within a residual layer from previous day(s) is entrained into the PBL, increasing ground-level $[O_3]$. This process continues until the PBL height reaches its peak. Simultaneously, ozone production starts with its precursor emissions in the presence of sunlight, a rate that increases with increasing sunlight intensity and surpasses the transport rate of $[O_3]$ by mid to late afternoon. Furthermore, Fig. 4 indicates that the peak time of $[O_3]$ differs between the CTRL run and the noAZ run at some locations for some days. These differences of $[O_3]$ peak time indicate the features of ozone transport.

25 Figure 5 displays the mean diurnal variation of $[O_3]$ for the different emission scenarios for the two cases. The data are averaged over all urban grid cells (i.e., not solely over the station sites presented in Fig. 4) in Phoenix for May 11–14, 2012, and 16–19 July 2005, respectively. The relative contribution of emissions to Phoenix $[O_3]$ are clear and the diurnal features similar to those shown in Fig. 4, emphasizing the crucial roles of both local and remote emissions.

**Regional-scale
transport of air
pollutants**

J. Li et al.

Title Page

Abstract

Introduction

Conclusions

References

Tables

Figures



Back

Close

Full Screen / Esc

Printer-friendly Version

Interactive Discussion



Regional-scale transport of air pollutants

J. Li et al.

Title Page

Abstract

Introduction

Conclusions

References

Tables

Figures



Back

Close

Full Screen / Esc

Printer-friendly Version

Interactive Discussion



The daily maximum 8 h average (DMA8) $[O_3]$ for different simulated emission scenarios (CTRL, BEO, SoCal, and AZ) is assessed at observation sites and all urban grid cells within Phoenix (Fig. 6). The model reproduces observations very well with a slight underestimation on 19 July 2005, and overestimation on 13 May 2012. Following Huang et al. (2013), the contribution of SoCal to DMA8 $[O_3]$ in the Phoenix area is the difference between the CTRL and noCA experiments, and ranges between 20–30 ppbv for the May case and 5–20 ppbv for the July case. Relative to the CTRL run, the percentage contributions of 26–36 % for the May case and 7–38 % for the July event emphasize the significant effect of southern California emissions on Phoenix metropolitan area air quality. For the two episode days, the contributions are 28 ppb (36 %) for 14 May 2012, and 11 ppb (16 %) for 19 July 2012.

The means of DMA8 $[O_3]$ throughout the Phoenix urban area (about 1100 grid cells) arising from the different emission scenarios are shown in Fig. 6b and d, and indicate similar values to those at observation sites (Fig. 6a and c). The contribution of SoCal emission to DMA8 $[O_3]$ for the Phoenix metropolitan area ranges between 20–32 ppbv for the 11–14 May 2012, case, and from 6–22 ppbv for the 16–19 July 2005, case. The percentages, relative to CTRL, are from 27 to 37 % for 11–14 May, and from 9 to 40 % for 16–19 July. Considering only the two days with the maximum ozone concentrations, the contributions are 29 ppb (37 %) and 11 ppb (16 %) for 14 May, and 19 July, respectively. Figure 6 demonstrates the following important results: (1) the impact of AZ emissions on DMA8 $[O_3]$ in the Phoenix area is greater than that of the SoCal's; (2) even so, SoCal emissions considerably increase DMA8 $[O_3]$ in the Phoenix area by up to 30 ppbv, though this is day and case dependent; (3) the DMA8 $[O_3]$ from the BEO experiment are in excess of 30 ppbv. In other words, the contribution of BEO emissions to Phoenix DMA8 $[O_3]$ cannot be ignored despite the region's aridity and relative lack of dense forests.

In summary, our results demonstrate that removing SoCal emissions would facilitate attainment of $[O_3]$ in Phoenix on some days, but not on others. In other words, SoCal emissions are an important, if uneven, contributor to the DMA8 $[O_3]$ exceedances

[O₃] differences for the July case also presents patterns of residual ozone with positive slopes indicating transport (Fig. 7b). These slopes are, however, less pronounced than the May case.

The data within each model vertical layer are examined. It is found that peak transport occurs in different model layers depending on the event. For the July event, there is ozone transport from the 5th model layer (about 150 m a.g.l.) to the 13th model layer. For the May event, ozone transport occurs from the 5th to 17th (2000 m a.g.l.) model layers. The Hovmoller diagrams for NO_x and VOCs indicate that most air masses of NO_x and VOCs are horizontally confined near emission source areas and are vertically restricted to below about 1500 m a.g.l. (figure not shown), compared to the magnitude presented in Fig. 7.

We next examine how pollutants from southern California are transported into south-central Arizona and discuss the physical-chemical mechanisms responsible. Analysis of anthropogenic emission distributions indicates that emissions mainly originate from coastal areas in southern California (also see their Fig. 1 in Chen et al., 2013 for emission distribution). Therefore, we first explain how the pollutants cross the coastal mountains and reach the inland desert regions in southern California.

As discussed in Sect. 1, wind fields are the principal factor in pollutant transport (Lee et al., 2007). Figure 8 displays the daytime averaged (20 Z to 02 Z) wind vector field at 40 m a.g.l. in the southern California coastal area of 16–19 July 2005. The wind patterns exhibit a combination of on-shore ocean breezes and mountain-induced upslope winds, similar to features reported by Lu and Turco (1996) and Lu et al. (1997). The wind field distribution shown in Fig. 8 propels pollutants emitted in coastal areas towards the coastal mountains. The polluted air masses can be lofted up to 3–4 km a.g.l. over the mountains through the Mountain Chimney Effect (MCE, Lu and Turco, 1996). The pollutants above mountain-top height might either be transported into the free atmosphere over the coast (Lu and Turco, 1996) and/or be transported towards the inland desert and affect the air quality in the desert of southern California (Huang

Regional-scale transport of air pollutants

J. Li et al.

Title Page

Abstract

Introduction

Conclusions

References

Tables

Figures



Back

Close

Full Screen / Esc

Printer-friendly Version

Interactive Discussion



et al., 2013; VanCuren 2014) and of nearby mountain states (Langford et al., 2010; Huang et al., 2013).

The entire transport path, from the southern California coast to south-central Arizona, and the associated ozone vertical distributions along cross-sections A'A, B'B, D'D and E'E, is addressed here in this subsection. First, vertical distributions of $[O_3]$ along cross-sections A'A and B'B are checked from 21 Z to 24 Z each day and Fig. 9 is an example of vertical distributions of $[O_3]$ along cross-section A'A and B'B at 22 Z on 17 July 2005. Results presented in Fig. 9 are similar to those reported by Lu and Turco (1996, in their Figs. 4 and 6) from modeling and Langford et al. (2010; in their Fig. 3) from observations, indicating the appropriate WRF-Chem simulation of the Mountain Chimney Effect (MCE). Note the distribution of potential temperature contours in Fig. 9, illustrating that ozone-laden air masses above mountain peak height may be directly transported into the desert PBL under appropriate flow at these levels. This pattern differs from that of transport back to the free atmosphere over coastal basins (note the tongue of high $[O_3]$ to the west of the peak in Fig. 9a). This is because of the particularly high PBL height (in excess of 3–4 km a.g.l.) in the desert during daytime due to strong solar radiation. At nighttime, ozone air masses subsequently reside in the residual layers and/or stable PBL in the desert, and are continuously advected by westerly winds (part of the near-surface ozone will be consumed by titration from NO_x and by deposition during nighttime). Importantly, Fig. 8 indicates the presence of strong winds from the coast flowing through the mountain passes. For example, there are southerly winds flowing along the Cajon Pass (see location in Fig. 1b) and strong westerly winds flowing along the San Gorgonio Pass (see location Fig. 1b), which are realistic and consistent with the immense fields of wind turbines there. With the wind pattern shown in Fig. 8, ozone in low air layers can be directly transported into the southern Mojave Desert Air Basin (SMDAB, See Fig. 1b) from the Greater Los Angeles Air Basin (GLAAB) through the Cajon Pass. Ozone can also be transported eastward to the Salton Sea Air Basin (SSAB) from the GLAAB through the San Gorgonio Pass and from the San Diego Air Basin (SDAB) through other passes (see Fig. 8 for the locations and wind vectors).

Regional-scale
transport of air
pollutants

J. Li et al.

Title Page

Abstract

Introduction

Conclusions

References

Tables

Figures



Back

Close

Full Screen / Esc

Printer-friendly Version

Interactive Discussion



To demonstrate the model performance in simulating $[O_3]$ in the passes, Fig. 10 presents the hourly comparison of $[O_3]$ between observations and simulations (CTRL) at Crestline, near the Cajon Pass, and Banning Airport, near the San Gorgonio Pass. Figure 10 shows that the simulations and the observations are comparable from 17 July to 19 July 2005. In Fig. 10, model simulations with 12 km resolution are also plotted to characterize resolution-dependency. It is clear that with higher-resolution, simulated results are improved above those of coarser resolution, a feature likely due to more accurate ozone transport through the passes.

Figure 11 shows the horizontal distribution of the integrated fluxes of ozone differences ($\int ([O_3]_{CTRL} - [O_3]_{noCA}) V_{CTRL} dz$) from the surface to 1400 m a.g.l. averaged from (a) 18 Z to 02 Z and (b) 03 Z to 17 Z, 16–20 July 2005 (data from the other case 11–15 May 2012 are similar). Figure 11 emphasizes two key aspects of this transport:

1. There were stronger fluxes in the mountain passes, especially in the San Gorgonio Pass, than any other location, indicating the important contributions of mountain passes to ozone transport. Most recently, VanCuren (2014), based on ozone observation data analysis, also suggests the importance of ozone transported into the MDAB through the passes and has confirmed our model results.
2. Ozone fluxes are present, originating from the coasts and mountains in southern California, extending southeastward along the SSAB and the SMDAB (Fig. 11b), crossing the California-Arizona border near the southern Lower Colorado River, then moving northeastward (Fig. 11b) along the Gila river basin, and finally reaching the Phoenix area.

The vertical distribution of pollutants is also evaluated along cross-section D'D in the Salton Sea Valley and cross-section E'E in the Gila River Valley (locations are labeled in Fig. 1b). Presenting vertical distributions of VOC, NO_x and O_3 along D'D on 18 July from CTRL, Fig. 12 depicts the transport processes of the pollutants from late afternoon to midnight, as indicated by the location of high concentration fronts. The NO_x masses are horizontally confined to below 1 km a.s.l. with concentrations of 5–15 ppbv.

**Regional-scale
transport of air
pollutants**

J. Li et al.

Title Page

Abstract

Introduction

Conclusions

References

Tables

Figures



Back

Close

Full Screen / Esc

Printer-friendly Version

Interactive Discussion



**Regional-scale
transport of air
pollutants**

J. Li et al.

Title Page

Abstract

Introduction

Conclusions

References

Tables

Figures



Back

Close

Full Screen / Esc

Printer-friendly Version

Interactive Discussion



VOC plumes are confined below 2 km a.s.l. with concentrations of 10–20 ppbv. We also evaluated the vertical distribution of VOC from the BEO emissions experiment: the vertical distribution is similar to the VOC shown in Fig. 12, but the concentrations are about 10 ppbv (figure not shown). In other words, there are about 10 ppbv of VOC that are transported from coastal anthropogenic emissions to this region. Similar to NO_x concentrations, the highest concentrations of VOC are near the ground surface.

Ozone vertical distributions reach up to 2–3 km a.s.l. with concentrations as high as 90 ppbv. The high [O₃] is centered 1–2 km a.s.l. during nighttime while [O₃] is low near ground-level due to the chemical titration by NO_x and dry deposition (Fig. 12). In other words, among the three pollutants, ozone is most “long-lived” and NO_x has the shortest span, which is consistent with their atmospheric chemistry and previous results (e.g., Lee and Fernando, 2013).

The diurnal variation of a pollutant is, in part, a consequence of diurnal variation of flow (the other principal influence is the diurnal variation of the emissions themselves). During daytime, southeasterly winds (valley winds) at lower layers in the northern Salton Sea basin hinder the pollutants from being transported southeastward along the Salton Sea Basin (See Figs. 11a and 8). Therefore, parts of the pollutants, transported from the GLAAB through the San Gorgonio Pass, accumulate over the northern Salton Sea basin (as shown at 01 Z in Fig. 12) while parts of the pollutants crossed the Little San Bernardino Mountains and reached the SMDAB due to upslope flow (see Figs. 11a and 8). During nighttime, basin-scale mountain downslope winds transport the pollutants southeastward along the SSAB basin (Figs. 11b and 12).

Figure 13 is similar to Fig. 12 but presents results for the cross-section E'E in the Gila River basin in Arizona (location shown in Fig. 1b) on 18 July. During this time period, although concentrations of pollutants were further decreasing along this transport pathway, the ozone transport phenomenon was still very clear along the Gila River basin due to the prevailing nighttime southwesterly winds (see Fig. 11). These southwesterly winds can result from either the low-level jet from the northern Gulf of California during monsoon season (e.g., since mid-July of the warm seasons, Adams and Comrie,

1997) or by the inertia from a remnant of daytime westerly winds during pre-monsoon season (e.g. before Mid-July in the warm seasons, Lee and Fernando, 2013). At about 18 Z, the ozone in the residual layer mixes with PBL ozone generated by local photochemical reactions, and finally affects the ground-level concentrations in Phoenix and its surrounding rural areas.

4 Conclusion

As with other cities, Phoenix's ozone concentrations on exceedance days can be attributed to local precursor emissions and the transport of ozone from remote regions. In this study, WRF-Chem at high-resolution (~ 1.333 km grid spacing) is employed to investigate surface ozone distributions in southern California and south-central Arizona for two selected Phoenix episodes. Model simulations have been compared with surface observations of hourly ozone, CO, NO_x and wind fields in southern California and Arizona. The results indicate that the WRF-Chem configuration in this study can adequately simulate the spatial distribution, the magnitude, and the variability of the observations. The modeled ozone concentrations ([O₃]) fall in the acceptance range recommended by EPA.

Three sensitivity studies have been conducted to separate the contributions of southern California anthropogenic emissions (SoCal), of the Arizona local anthropogenic emissions (AZ), and of the biogenic emissions to Phoenix [O₃] on the exceedance days: (1) running WRF-Chem as CTRL but excluding SoCal emissions (noCA), (2) running WRF-Chem as the Control simulation but excluding AZ emissions (noAZ) and (3) running WRF-Chem as the Control simulation but excluding all anthropogenic emissions in domain 4 areas, leaving the biogenic emissions only (BEO). Our simulations indicate that AZ emissions play the key role in formation of the elevated and non-elevated [O₃] in Phoenix for the selected cases (see Figs. 4–6). SoCal emissions contribute to DMA8 [O₃] in the Phoenix area, and this impact varies between 5–30 ppbv at distinct observation sites and from 6–32 ppbv throughout the urban setting. In addition, our

Regional-scale transport of air pollutants

J. Li et al.

Title Page

Abstract

Introduction

Conclusions

References

Tables

Figures



Back

Close

Full Screen / Esc

Printer-friendly Version

Interactive Discussion



model simulations indicate the effects of SoCal emissions on DMA8 [O₃] in Phoenix are location and event dependent, but not negligible. The effects of BEO contributions to Phoenix DMA8 [O₃] are also significant in spite of the region's aridity.

The time series of [O₃] of the relative contributions to Phoenix [O₃] from SoCal and AZ emissions exhibit a diurnal variation. During nighttime hours, the transported ozone increases [O₃] while local emissions consume it. The reverse occurs during afternoon hours when locally generated emissions predominate.

WRF-Chem's high resolution resolves all pertinent topographical features, especially the critical low-elevation mountain passes, capturing the pollutant transport through them. Therefore, the pollutant's (mainly ozone) transport pathway in the lower troposphere is identified: The pollutants (mainly ozone) are first transported to the southern Mojave Desert Air Basin (SMDAB) and the Salton Sea Air Basin (SSAB) through both the Mountain Chimney Effect (MCE) and Mountain Pass Channel Effect (PCE) during daytime, affecting DMA8 [O₃] in these two air basins. The following physical transport paths (based on the two events) are: the pollutants are first transported southeastward along the two air basins (the SSAB and the SMDAB) in CA during nighttime, then northeastward along the Gila River basin in AZ during nighttime, and finally reach the Phoenix area and mix with the local air mass by turbulent mixing during daytime. The entire transport path is determined by a combination of local and synoptic circulations.

Since the PBL height can extend in excess of 3–4 km a.g.l. in desert air basins, pollutants may be directly transported into the daytime desert PBL from coasts by both PCE and MCE. Therefore, regional transport in the desert is accomplished in the PBL (daytime), and residual layer and stable PBL (nighttime).

This study indicates that in evaluating local emission controls in Phoenix, one should consider emission controls outside Phoenix (i.e., regional controls) and account for the effects of biogenic emissions in addition to local release of pollutants. Not to do so would lead to false expectations of attaining the NAAQS ozone standard, especially when new standards are more stringent.

Regional-scale transport of air pollutants

J. Li et al.

Title Page

Abstract

Introduction

Conclusions

References

Tables

Figures



Back

Close

Full Screen / Esc

Printer-friendly Version

Interactive Discussion



Acknowledgements. This work has been funded by National Science Foundation grants EaSM-3 DMS 1419693, BTS-0215, EAR-1204774 and EF-1049251. We thank the Julie Ann Wrigley Global Institute of Sustainability at Arizona State University for valuable support. The authors appreciate the comments and suggestions from Steven Peckham (NOAA). Chun Zhao (PNNL) and Xiaohong Liu (University of Wyoming) have also shared their successful experiences with the first author.

References

- Ackermann, I., Hass, H., Memmesheimer, M., Ebel, A., Binkowski, F., and Shankar, U.: Modal aerosol dynamics model for Europe: development and first applications, *Atmos. Environ.*, 32, 2981–2999, 1998.
- Adams, D. and Cowrie, A.: The North American monsoon, *BAMS*, 78, 2198–2213, 1997.
- Anderson, H.: Air pollution and mortality: a history, *Atmos. Environ.*, 43, 143–152, doi:10.1016/j.atmosenv.2008.09.026, 2009.
- Ashmore, M.: Assessing the future global impacts of ozone on vegetation, *Plant Cell Environ.*, 29, 949–964, doi:10.1111/j.1365-3040.2005.01341.x, 2005.
- Avnery, S., Mauzeral, D., Liu, J., and Horwiz, W.: Global crop yield reductions due to surface ozone exposure: 1: Year of 2000 crop production losses and economic damage, *Atmos. Environ.*, 45, 2284–2296, 2011.
- Chameides, W., Li, X., Tang, X., Zhou, X., Luo, C., Kiang, C., St John, J., Saylor, R., Liu, S., Lam, K., Wang, T., and Giorgi, F.: Is ozone pollution affecting crop yields in China? *Geophys. Res. Lett.*, 26, 867–870, doi:10.1029/1999gl900068, 1999.
- Chen, D., Li, Q., Stutz, J., Mao, Y., Zhang, L., Pikelnaya, O., and Tsai, J.: WRF-Chem simulation of NO_x and O₃ in the LA Basin during CalNex 2010, *Atmos. Environ.*, 81, 421–432, 2013.
- Chen, F. and Dudhia, J.: Coupling an advanced land surface hydrology model with the Penn State NCAR MM5 modeling system. Part 1: Model implementation and sensitivity, *Mon. Weather Rev.*, 129, 569–585, 2001.
- Chen, F., Kusaka, H., Bornstein, R., Ching, J., Grimmond, C., Grossman-Clarke, S., Loridan, T., Manning, K., Martilli, A., Miao, S., Sailor, D., Salamanca, F., Taha, H., Tewari, M., Wang, X., Wyszogrodzki, A., and Zhang, C.: The integrated WRF/urban modeling system: develop-

Regional-scale transport of air pollutants

J. Li et al.

Title Page

Abstract

Introduction

Conclusions

References

Tables

Figures



Back

Close

Full Screen / Esc

Printer-friendly Version

Interactive Discussion



Regional-scale transport of air pollutants

J. Li et al.

Title Page

Abstract

Introduction

Conclusions

References

Tables

Figures



Back

Close

Full Screen / Esc

Printer-friendly Version

Interactive Discussion



ment, evaluation, and applications to urban environmental problems, *Int. J. Climatol.*, 31, 273–288, doi:10.1002/joc.2158, 2011.

Ek, M., Mitchell, B., Lin, K., Rogers, Y., Grunmann, E., Koren, P., Gayno, V., and Tarpley, J.: Implementation of Noah land surface model advances in the National Centers for Environmental Prediction operational mesoscale Eta model, *J. Geophys. Res.*, 108, 8851, doi:10.1029/2002JD003296, 2003.

Emmons, L. K., Walters, S., Hess, P. G., Lamarque, J.-F., Pfister, G. G., Fillmore, D., Granier, C., Guenther, A., Kinnison, D., Laepple, T., Orlando, J., Tie, X., Tyndall, G., Wiedinmyer, C., Baughcum, S. L., and Kloster, S.: Description and evaluation of the Model for Ozone and Related chemical Tracers, version 4 (MOZART-4), *Geosci. Model Dev.*, 3, 43–67, doi:10.5194/gmd-3-43-2010, 2010.

EPA: Guideline for Regulatory Application of the Urban Airshed Model, US EPA Report No. EPA-450/4-91-013, Office of Air Quality Planning and Standards, Technical Support Division, Research Triangle Park, North Carolina, USA, 1991.

EPA: National Ambient Air Quality Standards for Ozone, available at: <http://www.epa.gov/glo/pdfs/20141125proposal.pdf>, 2014.

Fast, J., Doran, J., and Shaw, W.: The evolution of the boundary layer and its effect on air chemistry in the Phoenix area, *J. Geophys. Res.*, 105, 22833–22848, 2000.

Fast, J., Zaveri, D., Bian, X., Chapman, E., and Easter, R.: Effect of regional-scale transport on oxidants in the vicinity of Philadelphia during the 1999 NE-OPS field campaign, *J. Geophys. Res.*, 107, 4307, doi:10.1029/2001JD000980, 2002.

Friedl, M. A., McIver, D. K., Hodges, F., Zhang, X. Y., Muchnoey, D., Strahler, A. H., Woodcock, C. E., Gopal, S., Schneider, A., Cooper, A., Baccini, A., Gao, F., and Schaaf, C.: Global land cover mapping from MODIS: algorithms and early results, *Remote Sens. Environ.*, 83, 287–302, 2002.

Ginoux, P., Chin, M., Tegen, I., Prospero, J., Holben, B., Dubovik, O., and Lin, S.-J.: Sources and global distributions of dust aerosols simulated with the GOCART model, *J. Geophys. Res.*, 106, 20255–20273, 2001.

Grell, G. A. and Devenyi, D.: A generalized approach to parameterizing convection combining ensemble and data assimilation techniques, *Geophys. Res. Lett.*, 29, 38-1–38-4, doi:10.1029/2002GL015311, 2002.

**Regional-scale
transport of air
pollutants**

J. Li et al.

Title Page

Abstract

Introduction

Conclusions

References

Tables

Figures



Back

Close

Full Screen / Esc

Printer-friendly Version

Interactive Discussion



- Grell, G. A., Peckham, S. E., Schmitz, R., McKeen, S. A., Frost, G., Skamarock, W. C., and Eder, B.: Fully coupled “online” chemistry within the WRF model, *Atmos. Environ.*, 39, 6957–6975, doi:10.1016/j.atmosenv.2005.04.027, 2005.
- Gross, A. and Stockwell, W. R.: Comparison of the EMEP, RADM2 and RACM mechanisms, *J. Atmos. Chem.*, 44, 151–170, 2003.
- Guenther, A., Karl, T., Harley, P., Wiedinmyer, C., Palmer, P. I., and Geron, C.: Estimates of global terrestrial isoprene emissions using MEGAN (Model of Emissions of Gases and Aerosols from Nature), *Atmos. Chem. Phys.*, 6, 3181–3210, doi:10.5194/acp-6-3181-2006, 2006.
- He, H., Stehr, J. W., Hains, J. C., Krask, D. J., Doddridge, B. G., Vinnikov, K. Y., Canty, T. P., Hosley, K. M., Salawitch, R. J., Worden, H. M., and Dickerson, R. R.: Trends in emissions and concentrations of air pollutants in the lower troposphere in the Baltimore/Washington airshed from 1997 to 2011, *Atmos. Chem. Phys.*, 13, 7859–7874, doi:10.5194/acp-13-7859-2013, 2013.
- Hovmoller, E.: The trough-and-ridge diagram, *Tullus*, 1, 62–66, 1949.
- Huang, M., Bowman, K., Carmichael, G., Pierce, B., Worden, H., Lou, M., Cooper, O., Pollack, I., Ryerson, T., and Brown, S.: Impact of Southern California anthropogenic emissions on ozone pollution in the mountain states: model analysis and observational evidence from space, *J. Geophys. Res.-Atmos.*, 118, 12784–12803, 2013.
- IPCC: Climate change: the physical science basis, in: Fourth Assessment Report (AR4) of the Intergovernmental Panel on Climate Change, contribution of Working Group I, 996 pp., 2007.
- Kemball-Cook, S., Parrish, D., Ryerson, T., Nopmongkol, U., Johnson, J., Tai, E., and Yarwood, G.: Contributions of regional transport and local sources to ozone exceedances in Houston and Dallas: comparison of results from a photochemical grid model to aircraft and surface measurement, *J. Geophys. Res.*, 114, D00F02, doi:10.1029/2008JD010248, 2009.
- Klich, C. A. and Fuelberg, H. E.: The role of horizontal model resolution in assessing the transport of CO in a middle latitude cyclone using WRF-Chem, *Atmos. Chem. Phys.*, 14, 609–627, doi:10.5194/acp-14-609-2014, 2014.
- Langford, A., Senff, C., Alvarez, R., Banta, R., and Hardesty, R.: Long-range transport of ozone from the Los Angeles Basin: a case study, *Geophys. Res. Lett.*, 37, L06807, doi:10.1029/2010GL042507, 2010.
- Lee, S. and Fernando, H.: Dispersion of an urban photochemical plume in Phoenix metropolitan area, *Atmos. Environ.*, 80, 152–160, 2013.

Regional-scale transport of air pollutants

J. Li et al.

Title Page

Abstract

Introduction

Conclusions

References

Tables

Figures



Back

Close

Full Screen / Esc

Printer-friendly Version

Interactive Discussion



- Lee, S., Fernando, H., Princevac, M., Zajic, D., Sinesf, M., Mcculley, J., and Anderson, J.: Transport and diffusion of ozone in the nocturnal and morning planetary boundary layer of the Phoenix Valley, *Environ. Fluid Mech.*, 3 331–362, 2003.
- Lee, S. H., Fernando, H., and Grossman-Clarke, S.: MM5-SMOKE-CMAQ as a modeling tool for 8 h ozone regulatory enforcement: application to the state of Arizona, *Environ. Model. Assess.*, 12, 63–74, 2007.
- Levy II, H., Mahlman, J., Moxim, W., and Liu, S.: Tropospheric ozone: the role of transport, *J. Geophys. Res.*, 90, 3753–3772, 1985.
- Li, J., Georgescu, M., Hyde, P., Mahalov, A., and Moustauoui, M.: Achieving accurate simulations of urban impacts on ozone at high resolution, *Environ. Res. Lett.*, 9, 114019, doi:10.1088/1748-9326/9/11/114019, 2014.
- Lin, M., Fiore, A., Horowitz, L., Cooper, O., Naik, V., Holloway, J., Johnson, B., Middlebrook, A., Oltmans, S., Pollack, I., Ryerson, T., Warner, J., Wiedinmyer, C., Wilson, J., and Wyman, B.: Transport of Asian ozone pollution into surface air over the western United States in spring, *J. Geophys. Res.*, 117, D00V07, doi:10.1029/2011JD016961, 2012.
- Lin, Y. L., Farley, R. D., and Orville, H. D.: Bulk parameterization of the snow field in a cloud model, *J. Climate Appl. Meteor.*, 22, 1065–1092, 1983.
- Lu, R. and Turco, R.: Air pollution transport in a coastal environment. Part 2: Three-dimensional simulations of sea-breeze and mountain effect, *Atmos. Environ.*, 29B, 1499–1518, 1995.
- Lu, R. and Turco, R.: Ozone distributions over the Los Angeles Basin: three-dimensional simulations with the SMOG model, *Atmos. Environ.*, 30, 4155–4176, 1996.
- Lu, R., Turco, R., and Jacobson, M.: An integrated air pollution modeling system for urban and regional scales. Part 2: Simulations for SCAQS 1987, *J. Geophys. Res.*, 102, 6081–6098, 1997.
- MacDonald, C., Miller, D., and Raffuse, D.: Regional and local contributions to peak local ozone concentrations in six western cities, Final Report for Western States Air Resources Council (WESATR), STI-906004-2970-FR, Sonoma Technology, Inc. (www.sonomatech.com), 2006.
- Mauzerall, D. and Wang, X.: Protecting agricultural crops from the effects of tropospheric ozone exposure: reconciling science and standard setting in the United States, Europe, and Asia, *Annu. Rev. Energ. Env.*, 26, 237–268, 2001.
- Mesinger F., DiMego, G., Kalney, E., Mitchell, K., Shafran, P., Ebisuzaki, W., Jovic, D., Woollen J., Rogers, E., Berbery, E., Ek, M., Fan, Y., Grumbine, R., Higgins, W., Li, H., Lin, Y., Manikin,

Regional-scale transport of air pollutants

J. Li et al.

Title Page

Abstract

Introduction

Conclusions

References

Tables

Figures



Back

Close

Full Screen / Esc

Printer-friendly Version

Interactive Discussion



G., Parrish, D., and Shi, W.: North American regional reanalysis, *B. Am. Meteorol. Soc.*, 87, 343–360, 2006.

Mlawer, E. J., Taubman, S. J., Brown, P. D., Iacono, M. J. and Clough, S. A.: Radiative transfer for inhomogeneous atmospheres: RRTM, a validated correlated- k model for the longwave, *J. Geophys. Res.-Atmos.*, 102, 16663–16682, 1997.

Moore, T.: Ozone 301, Maricopa County Air Quality Department, 4 September 2014, available at: <http://www.wrapair2.org/WestJumpAQMS.aspx>, 2014.

Nunnermacker, L., Weinstein-Lloyd, J., Kleinman, L., Daum, P., Lee, Y., Springston, S., Klotz, P., Newman, L., Neuroth, G., and Hyde, P.: Ground-based and aircraft measurements of trace gases in Phoenix, Arizona (1998), *Atmos. Environ.*, 38, 4941–4956, 2004.

Peckam, S., Grell, G., McKeen, S., Ahmadov, R., Barth, M., Pfister, G., Wiedinmyer, C., Fast, J., Gustafsson, W., Ghan, S., Zaveri, R., Easter, R., Barnard, J., Chapman, E., Hewson, M., Schmitz, R., Salzmann, M., Beck, V., Freitas, S., Previsao de, C., and Estudos, T.: WRF/CHEM Version 3.5 User's Guide, available at: ruc.noaa.gov/wrf/WG11/Users_guide.pdf (last access: 12 February 2013).

Pusede, S. E. and Cohen, R. C.: On the observed response of ozone to NO_x and VOC reactivity reductions in San Joaquin Valley California 1995–present, *Atmos. Chem. Phys.*, 12, 8323–8339, doi:10.5194/acp-12-8323-2012, 2012.

Schell, B., Ackermann, I., Hass, H., Binkowski, F., and Ebel, A.: Modeling the formation of secondary organic aerosol with a comprehensive air quality modeling system, *J. Geophys. Res.*, 106, 28275–28293, 2001.

Skamarock, W., Klemp, J., Dudhia, J., Gill, D., Barker, D., Wang, W., and Powers, J.: A description the Advanced Research WRF version 3, available at: www2.mmm.ucar.edu/wrf/users/docs/arw_v3.pdf, 2008.

Smith, K., Jerrett, M., Anderson, R., Burnett, R., Stone, V., Derwent, R., Atkinson, R., Cohen, A., Shonkoff, S., Krewski, D., Pope, III, A., Thun, M., and Thurston, G.: Public benefits of strategies to reduce greenhouse-gas emissions: health implications of short-lived greenhouse pollutants, *Lancet*, 374, doi:10.1016/S0140-6737(09)61716-5, 2009.

Stock, Z. S., Russo, M. R., and Pyle, J. A.: Representing ozone extremes in European megacities: the importance of resolution in a global chemistry climate model, *Atmos. Chem. Phys.*, 14, 3899–3912, doi:10.5194/acp-14-3899-2014, 2014.

Stockwell, W. R., Middleton, P., Chang, J. S., and Tang, X.: The second generation regional acid deposition model chemical mechanism for regional air quality modeling, *J. Geophys. Res.*, 95, 16343–16367, 1990.

Taha, H: Urban surface modification as a potential ozone air-quality improvement strategy in California: a mesoscale modeling study, *Bound.-Lay. Meteorol.*, 127, 219–239, 2008.

Tie, X., Brasseur, G., and Ying, Z.: Impact of model resolution on chemical ozone formation in Mexico City: application of the WRF-Chem model, *Atmos. Chem. Phys.*, 10, 8983–8995, doi:10.5194/acp-10-8983-2010, 2010.

Zhao, C., Liu, X., Leung, L. R., Johnson, B., McFarlane, S. A., Gustafson Jr., W. I., Fast, J. D., and Easter, R.: The spatial distribution of mineral dust and its shortwave radiative forcing over North Africa: modeling sensitivities to dust emissions and aerosol size treatments, *Atmos. Chem. Phys.*, 10, 8821–8838, doi:10.5194/acp-10-8821-2010, 2010.

Zhao, C., Liu, X., and Leung, L. R.: Impact of the Desert dust on the summer monsoon system over Southwestern North America, *Atmos. Chem. Phys.*, 12, 3717–3731, doi:10.5194/acp-12-3717-2012, 2012.

Regional-scale transport of air pollutants

J. Li et al.

Title Page

Abstract

Introduction

Conclusions

References

Tables

Figures



Back

Close

Full Screen / Esc

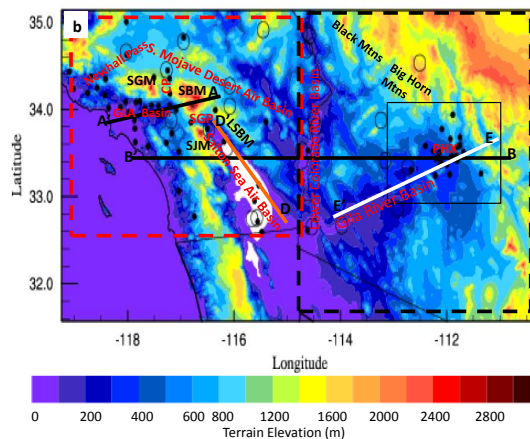
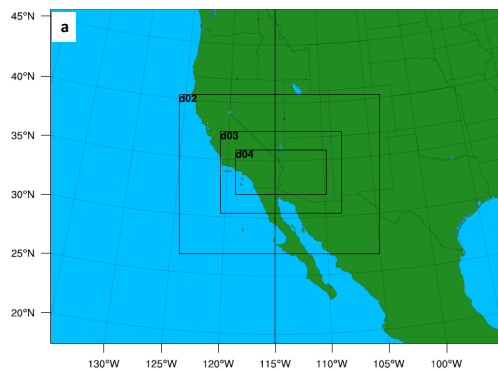
Printer-friendly Version

Interactive Discussion



Regional-scale transport of air pollutants

J. Li et al.



Title Page

Abstract Introduction

Conclusions References

Tables Figures

◀ ▶

◀ ▶

Back Close

Full Screen / Esc

Printer-friendly Version

Interactive Discussion



Regional-scale
transport of air
pollutants

J. Li et al.

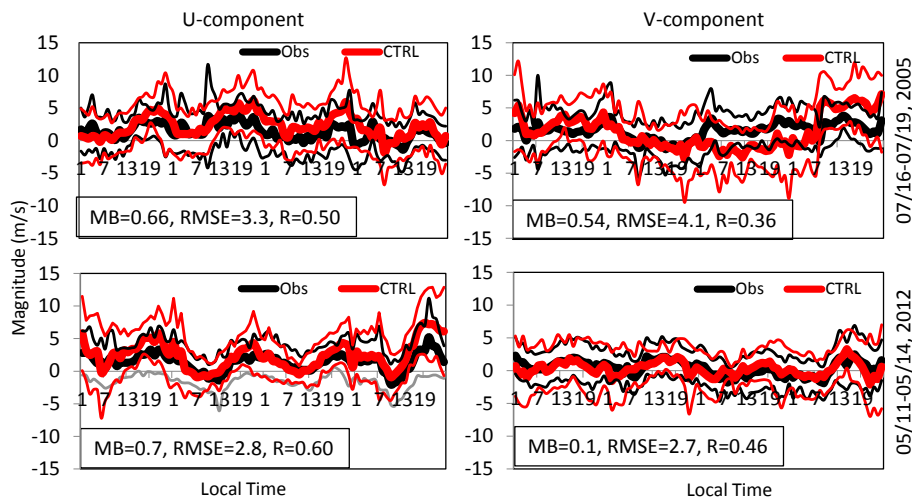


Figure 2. Surface wind comparisons between simulations (bold-red) and observations (bold black). There are totally 20 sites, including those in CA and AZ with locations shown in Fig. 1b as circles. The variation ranges of simulation and observation are correspondently labeled by thin-red-line and thin-black-line, respectively. Mean Biases (MB), RMSE and correlation coefficient (R) are labeled also. CTRL represents WRF-Chem control run.

Regional-scale
transport of air
pollutants

J. Li et al.

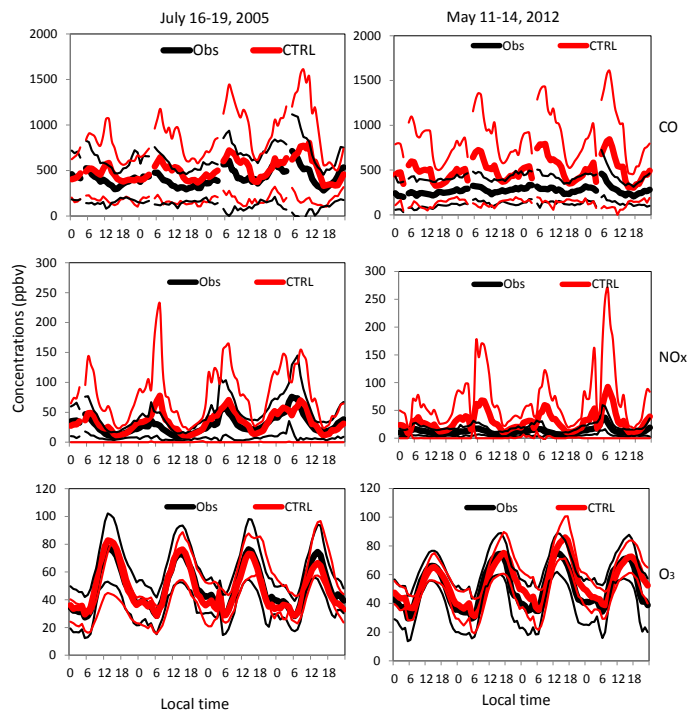


Figure 3. The comparisons of CO, NO_x, and O₃ concentrations between observations (bold black) and simulations (bold red) in Domain 4. There are 23 sites for NO_x, 20 sites for CO, and 65 sites for O₃ observations during the study time periods. The locations are shown in Fig. 1b. The variation ranges of simulation and observation are correspondently labeled by thin-red-line and thin-black-line, respectively. Missing observation time (4:00 LT) is masked in the figure. CTRL represents WRF-Chem control run.

Title Page

Abstract

Introduction

Conclusions

References

Tables

Figures



Back

Close

Full Screen / Esc

Printer-friendly Version

Interactive Discussion



Regional-scale
transport of air
pollutants

J. Li et al.

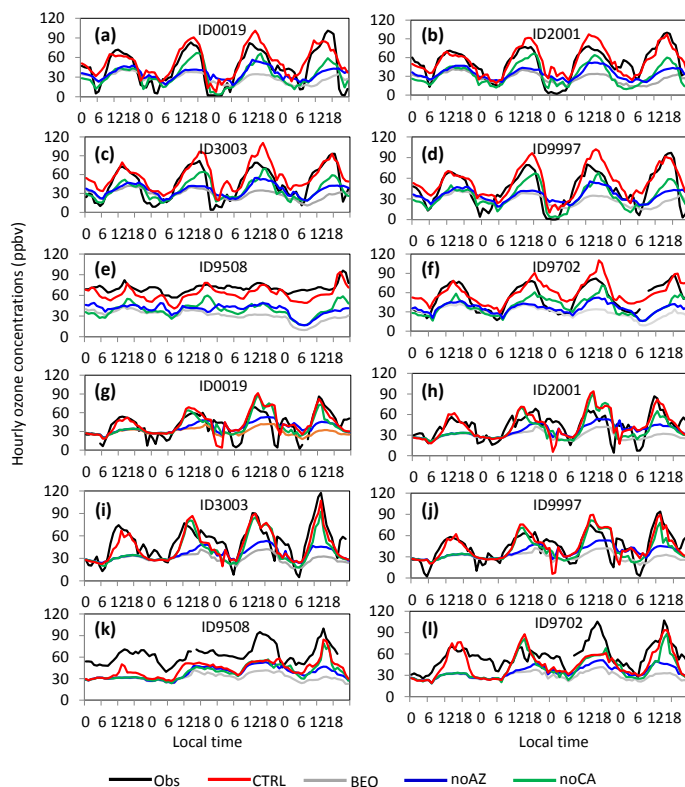


Figure 4. Relative contributions of different emission scenarios to $[O_3]$ at observation sites in Phoenix metropolitan area and surrounding rural areas. The dates are 11–14 May 2012 (**a–f**) and 16–19 July 2005 (**g–l**). Idxxxx corresponds to the EPA AIRS site number in Maricopa County, Arizona. Black line indicates the $[O_3]$ observation. Red line represents the simulated $[O_3]$ for the CTRL run. Blue line shows the $[O_3]$ for the noAZ run. Green line displays the $[O_3]$ for the noCA run. Gray line is the $[O_3]$ for the BE0 run.

Title Page

Abstract

Introduction

Conclusions

References

Tables

Figures



Back

Close

Full Screen / Esc

Printer-friendly Version

Interactive Discussion



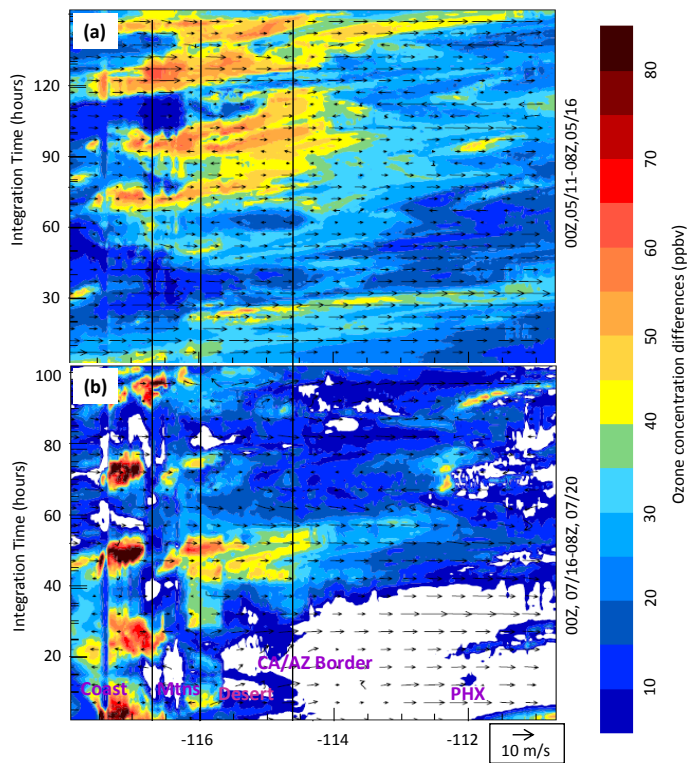


Figure 7. Hovmoller diagram of $[O_3]$ differences (CTRL minus noCA) at 13th vertical model layer (about 1100 m a.g.l.) along the cross-section B'B shown in Fig. 1b for July case (top) and May case (bottom). Approximate locations of Phoenix (PHX), desert, mountains (Mnts), and coast are also labeled in Fig. 7. The integrating is counted from 00Z, 10 May 2012, and 00Z, 15 July 2005, respectively.

Regional-scale transport of air pollutants

J. Li et al.

| | |
|--------------------------|--------------|
| Title Page | |
| Abstract | Introduction |
| Conclusions | References |
| Tables | Figures |
| ◀ | ▶ |
| ◀ | ▶ |
| Back | Close |
| Full Screen / Esc | |
| Printer-friendly Version | |
| Interactive Discussion | |



Regional-scale transport of air pollutants

J. Li et al.

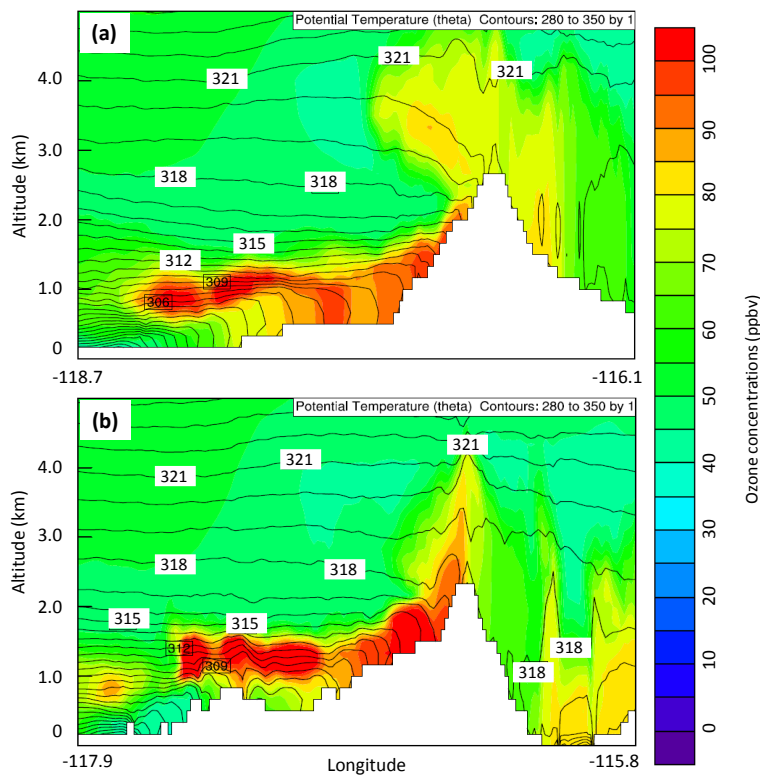


Figure 9. Vertical distributions of ozone along cross-section A'A (a) and B'B (b) shown in Fig. 1b at 22 Z of July, 17, 2005. The contours are potential temperature starting at 280 K with 1 K interval.

Regional-scale
transport of air
pollutants

J. Li et al.

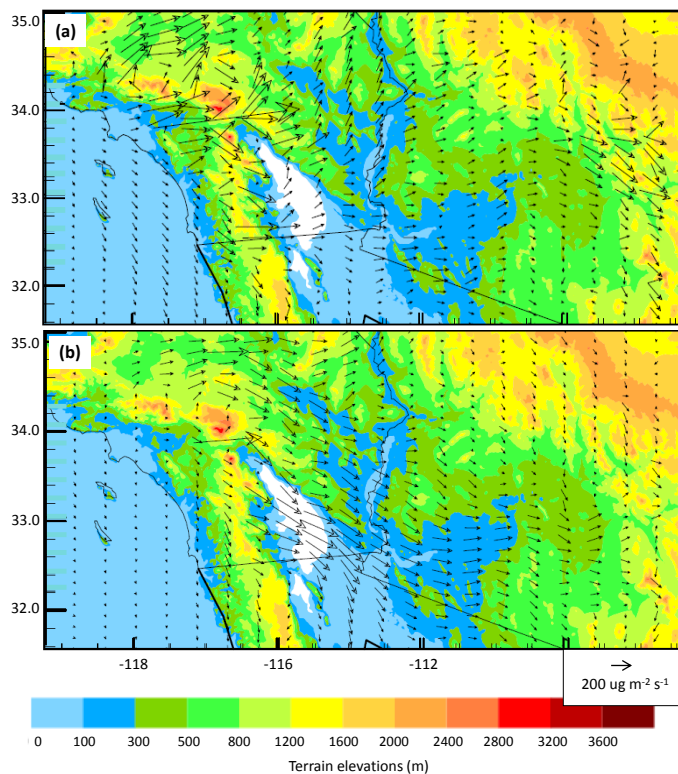


Figure 11. Integrated fluxes of ozone differences (CTRL-noCA) from surface to 1400 m a.g.l.: (a) average from 18 Z to 02 Z, 16 July to 20 July 2005, and (b) average from 03 Z to 17 Z, 16 July to 20 July 2005.

Title Page

Abstract

Introduction

Conclusions

References

Tables

Figures

◀

▶

◀

▶

Back

Close

Full Screen / Esc

Printer-friendly Version

Interactive Discussion



Regional-scale transport of air pollutants

J. Li et al.

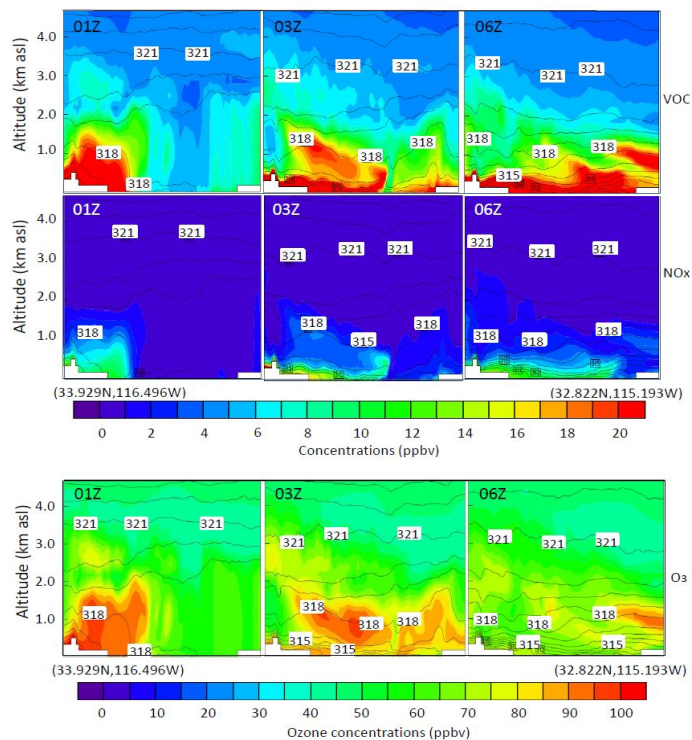


Figure 12. The vertical distribution of VOC (top), NO_x (middle), and O₃ (bottom) along the cross-section D'D (shown in Fig. 1b) in Salton Sea Basin at 01 Z, 03 Z, and 06 Z, 18 July 2005. Contours are potential temperature with 1 K interval.

Title Page

Abstract Introduction

Conclusions References

Tables Figures

◀ ▶

◀ ▶

Back Close

Full Screen / Esc

Printer-friendly Version

Interactive Discussion



Regional-scale
transport of air
pollutants

J. Li et al.

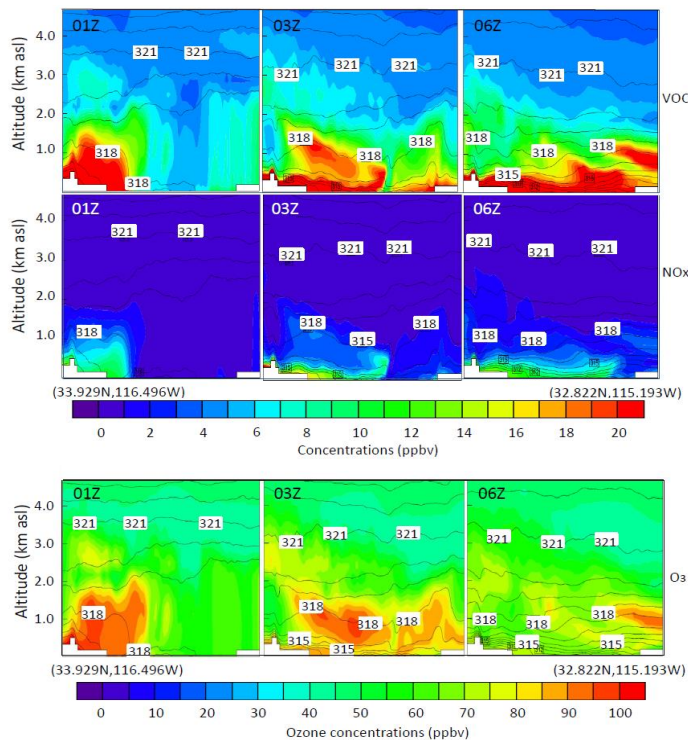


Figure 13. The vertical distribution of VOC (top), NO_x (middle), and O_3 (bottom) along the cross-section D'D (shown in Fig. 1b) in Gila River Basin, Arizona at 05Z, 11Z, and 18Z, 18 July 2005. Contours are potential temperature with 1 K interval.

Title Page

Abstract

Introduction

Conclusions

References

Tables

Figures

◀

▶

◀

▶

Back

Close

Full Screen / Esc

Printer-friendly Version

Interactive Discussion

